Received: 4 March 2022 | Revised: 17 May 2022 | Accepted: 4 July 2022

DOI: 10.1002/mop.33415

RESEARCH ARTICLE

WILEY

A wideband isolation technique using bezel coupled T-type isolator for smartwatch MIMO applications

Babar A. Baloch[1] | **Longyue Qu**[2] | **Zeeshan Zahid**[1] | **Adnan A. Khan**[1]

[1]Department of Electrical Engineering, Military College of Signals, National University of Sciences and Technology, Islamabad, Pakistan

[2]Department of Electronics and Information Engineering, Harbin Institute of Technology, Shenzhen, China

Correspondence
Zeeshan Zahid, Department of Electrical Engineering, Military College of Signals, National University of Sciences and Technology, Islamabad, Pakistan.
Email: zeeshanzahid@mcs.edu.pk

Abstract

This letter presents a wideband bezel coupled T-type isolator, decoupling two antenna elements for smartwatch multiple-input multiple-out applications. The antenna elements consist of PIFA antennas operating at 2.45 GHz, covering Bluetooth and Wi-Fi bands. The proposed T-type isolator has been installed between the antenna elements made by inserting two slits in the bezel separated by 21 mm. The separated segment of the bezel is connected with the circular ground plane by a conducting strip and an inductor. In this way, the slits offer stray capacitance, and the capacitive coupling between the T-type isolator has been utilized to achieve a wide isolation bandwidth. Meanwhile, the isolation can also be tuned using the gaps of the slits and the inductor. The design performance has been validated in simulations and measurement. The measured impedance bandwidth is higher than 120 MHz whereas the isolation bandwidth is 790 MHz with a maximum isolation higher than 22 dB. The measured envelop correlation coefficient is below 0.01. The proposed design is a good candidate for smartwatch applications.

KEYWORDS

coupling, isolator, multiple-input multiple-out, smartwatch, wideband isolation

1 | INTRODUCTION

Recently, wearable technology has gained enormous attention due to its capability in offering a hand-free way to communicate data. Among wearable devices, smartwatches are the most popular ones, having have gain enormous attention due to attractive applications such as trekking, health monitoring, fitness training, and so on. Data communication is carried out between smartwatches and other devices on Wi-Fi and GPS bands.[1] To meet the emerging market requirements of smart and efficient antennas for smartwatch applications working in GPS and Wi-Fi bands, a range of designs have been proposed.[2–6] Antennas in smartwatches are accompanied by harsh requirements and challenging implementation circumstances operate in a very challenging environment due to the proximity of human body as human tissues severely affect the antenna performance.[7] Furthermore, body movements result in shadowing and scattering and thereby causing channel fading despite using a high impedance surface.[8] To achieve reliable communication link and to mitigate channel path-loss, multiple-input multiple-output (MIMO) technology is essential to meet smartwatch applications.[9] Herein, high isolation and low correlation are important features to guarantee the MIMO performance, which could be easily achieved by disposing of the antenna elements at a large distance. However, compact sizes of smartwatches are much smaller as compared to smartphones and USB dongles, which poses another design challenge to smartwatch MIMO antennas resulting in strong mutual coupling.

Accordingly, various designs for smartwatch MIMO applications have been proposed in the literature.[10–14]

To achieve high port-to-port isolation covering a wideband frequency range, characteristic mode theory was utilized in Wen et al.[10] The characteristic mode theory is used to excite degenerate modes by employing ground modification and orthogonal T-shaped monopoles. However, the geometry lacks coplanar design requirements. Polarization diversity was employed in a two-port system using smartwatch annular integrated ring.[11] Dual-polarized colocated slots were etched on a wedge profile cavity[12,13] and a cuboid cavity[14] to achieve polarization diversity resulting in higher isolation for wider bandwidth. However, the design is unsuitable for low-profile smartwatch applications. Although wideband isolation in a dual-port antenna was demonstrated in Li et al.,[15] the complex feed structure is unsuitable for smartwatch applications. PIFA-based MIMO antennas were proposed without isolator in Chen et al.[16] and Woo et al.,[17] but the large-sized antennas are impractical in smartwatches. Therefore, there is a desperate demand for compact geometry, wideband isolation, ease of integration and fabrication in modern smartwatches. Ground radiation antenna (GradiAnt) is a coplanar antenna suitable for mobile device operation.[18–20] However, narrow isolation bandwidth has been a major drawback in GradiAnt-based MIMO antennas proposed in Qu and colleagues.[21–23] Many bandwidth enhancement techniques have been reported in the literature that can be employed to enhance the bandwidth of the PIFA antenna.[24,25] However, the techniques focused on isolation bandwidth enhancement need further investigation.

In this letter, a PIFA-based MIMO antenna solution has been proposed for smartwatch applications with a bezel-coupled isolator for wideband isolation. The isolator consists of a segmented bezel attached externally to the ground plane through a metallic strip and a lumped inductor. The capacitive coupling between the isolator and the larger bezel has been controlled by the gaps to achieve wideband isolation performance. Furthermore, the isolator is tunable using the isolation inductor.

2 | ANTENNA CONFIGURATION AND OPERATION MECHANISM

The geometry of the proposed smartwatch MIMO antenna is shown in Figure 1. A circular ground plane with a diameter of 42 mm is etched on the FR-4 substrate ($\varepsilon_r = 4.4$, $\tan(\delta) = 0.02$, thickness 1 mm). The ground plane is surrounded by a circular metallic bezel with a diameter and height 48 and 5 mm, respectively. PIFA elements are installed orthogonal to each other, that is, at

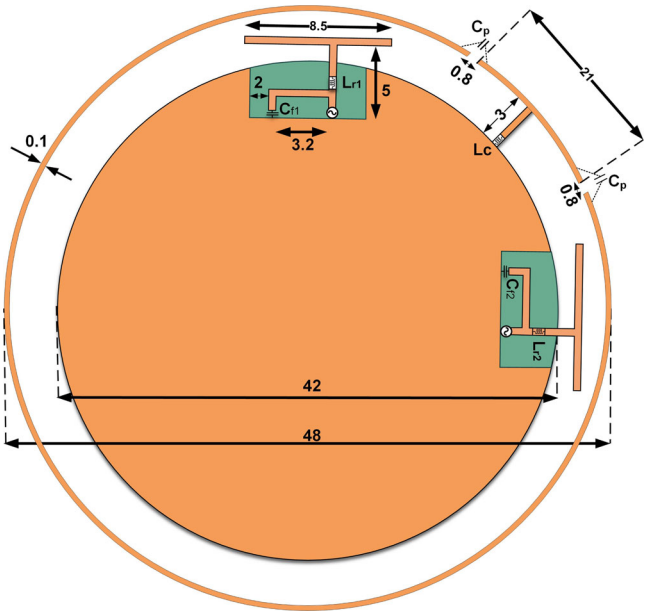

FIGURE 1 Geometry of the proposed MIMO antenna

the right and top edges of the circular ground plane. The antenna elements are designed by etching an $8 \times 4\ mm^2$ sized clearance in the circular ground plane. The radiating PIFA antenna contains the resonance inductor (L_r), that is used to tune the operating frequency. The size of the feed loop is $5 \times 2.5\ mm^2$ containing the feed capacitor (C_f), for impedance matching control. The arc length of the segmented bezel used in the T-shape isolator is 21 mm whereas the gaps on either side of the segmented bezel is 0.8 mm. The segment is connected with the ground place with a conducting strip and an isolation inductor (L_c).

The operation mechanism of the proposed MIMO antennas can be explained using the theory of microwave networks. The MIMO system can be represented as a three-port network with the isolator port terminated at an inductive load Z_L. The reflection coefficient Γ at the isolator terminal is defined as

$$\Gamma = \frac{V_3^-}{V_3^+} = \frac{Z_L - Z_o}{Z_L + Z_o}, \tag{1}$$

where Z_o represents the characteristic impedance. The network can be modeled as a 3×3 S-matrix. According to the decoupling theorem,[26,27] the coupling between the antenna elements in the presence of the isolator can be expressed as,[21]

$$S'_{12} = S_{12} + \frac{S_{13}S_{23}\Gamma}{1 - \Gamma S_{33}}, \tag{2}$$

where S'_{12} and S_{12} represent coupling coefficients between the antenna elements with and without the

loop-type isolator, respectively. In Equation (2), S_{13} represents the mutual coupling between Antenna 1 (Port 1) and the isolator (Port 3), and S_{23} represents the mutual coupling between Antenna 2 (Port 2) and the isolator (Port 3). Equation (2) indicates that the isolator plays an important role in achieving critical isolation, that is, $S'_{12}=0$. Usually, the isolation bandwidth is predetermined by the Q-factor of the isolator, so that a high-Q isolator can only operate within a limited bandwidth, which is the case reported in the literature. To achieve wideband isolation, the coupling between the isolator and the conducting structure is of paramount importance. In the proposed case the capacitive coupling between the T-type isolator and the segmented bezel has been exploited. The isolator being electrically small (a higher-Q structure) capacitively couples with the electrically large (lower-Q) bezel providing wideband isolation. This is the fundamental principle behind the proposed technique.

3 | SIMULATION RESULTS

The reference design has been designated as the orthogonal PIFA elements without the isolator for performance comparison. Full-wave simulations were conducted to observe the performance of the proposed MMO antenna design. In the reference design without any isolator, the simulated values of L_{r1}, C_{f1}, L_{r2}, and C_{f2} of both antenna elements were 8 nH, 0.55 pF, 7.5 nH and 0.38 pF, respectively. In the proposed design with the T-type isolator, the optimized values of L_{r1}, C_{f1}, L_{r2}, C_{f2}, and L_c were 7 nH, 0.55 pF, 7.5 nH, 0.85 pF, and 1.85 nH, respectively. Even though the structures of antenna elements are identical, the optimized values of the lumped components are different. The reason behind the difference is the asymmetry of antenna structure with reference to the location of the isolator. In the case of Antenna 1, the feed loop is placed behind the radiator with reference to the isolator whereas in the case of Antenna 2, the feed loop is placed closer to the isolator. Further, it was observed that if Antenna 1 is flipped so that the feed loop is closer to the isolator, the values of lumped components become identical.

Figure 2A,B show the simulated S-parameters of the reference design and the proposed design, respectively. For the reference design, it can be observed that the matching bandwidth of both antenna elements is 130 MHz (2.38–2.51 GHz) with reference to −10 dB, and the peak isolation (10 dB) is observed at 2.46 GHz. In the case of the proposed design, the impedance bandwidth of Antenna 1 and 2 are 130 MHz (2.38–2.51 GHz) and 110 MHz (2.38–2.51 GHz), respectively, as shown in Figure 2. Wideband isolation of 650 MHz (2.15–2.8 GHz) with reference to −20 dB is observed with peak isolation of −47 dB at 2.45 GHz. In particular, the mutual coupling within the Bluetooth/Wi-Fi band is less than −25 dB.

Wide isolation bandwidth is achieved by tuning the isolation inductor and adjusting the gaps between the isolator and the bezel. The impact of the gaps and the inductor on the isolation performance have been presented in Figure 3. Figure 3A presents the effect of increasing the gaps in the slots of the bezel. The gaps determine the parasitic capacitance between the T-type isolator and the larger bezel. Increasing the gap decreases the parasitic capacitance, shifting the isolation curve toward higher frequencies. It is evident that the optimum value of the gap is 0.8 mm producing wideband isolation. Figure 3B presents the effect of increasing the arc length (separation between the slits) that has a strong impact on the isolation performance. The isolation was improved as the length was increased from 17 to 21 mm. The isolation degrades with further increase in the length. The inductor L_c plays a significant role in adjusting the isolation, and its effect can be clearly seen in Figure 3C when the values of L_c were increased from 1.6 to 2 nH. It

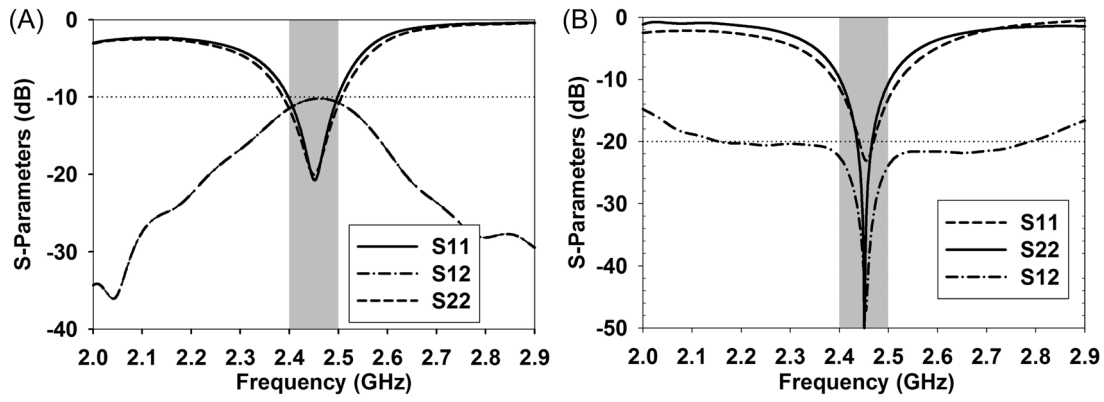

FIGURE 2 Simulated S-parameters of (A) reference antenna and (B) proposed antenna.

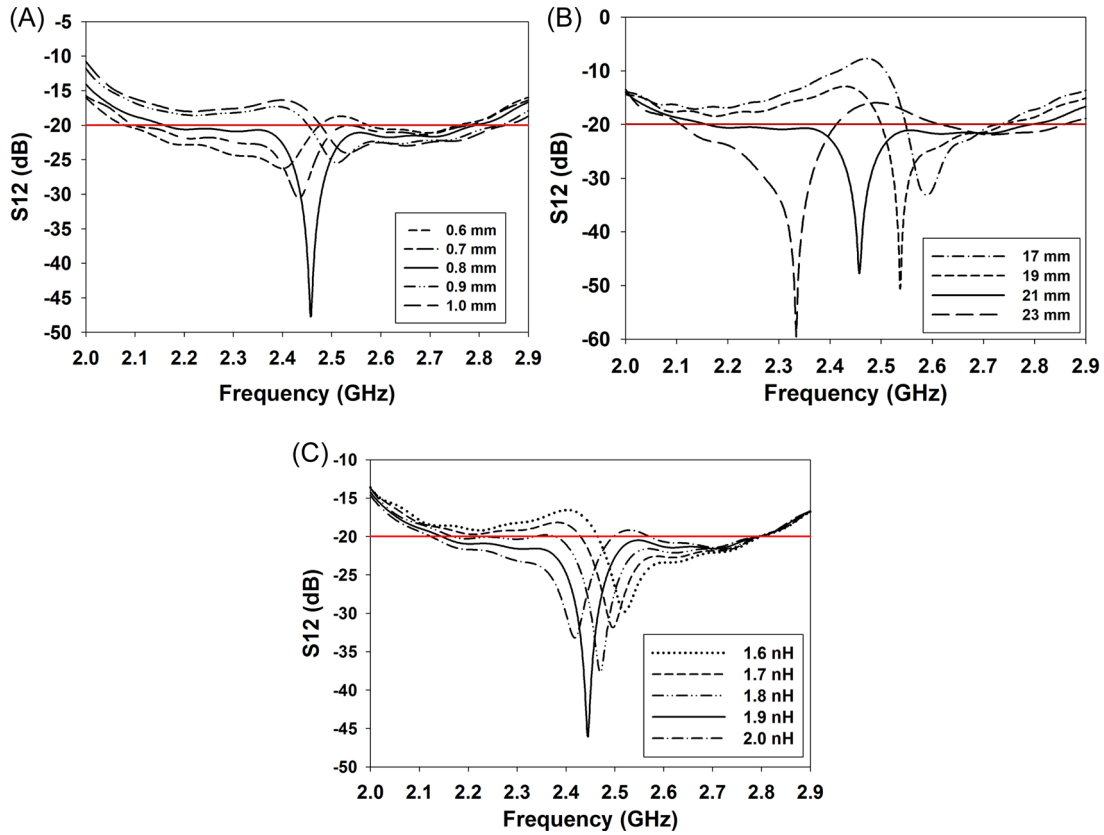

FIGURE 3 Parametric analysis of the antenna by varying (A) slot gaps in the bezel, (B) arc length of isolator, and (C) inductor L_c.

FIGURE 4 (A) Fabricated antenna and (B) measured S-parameters.

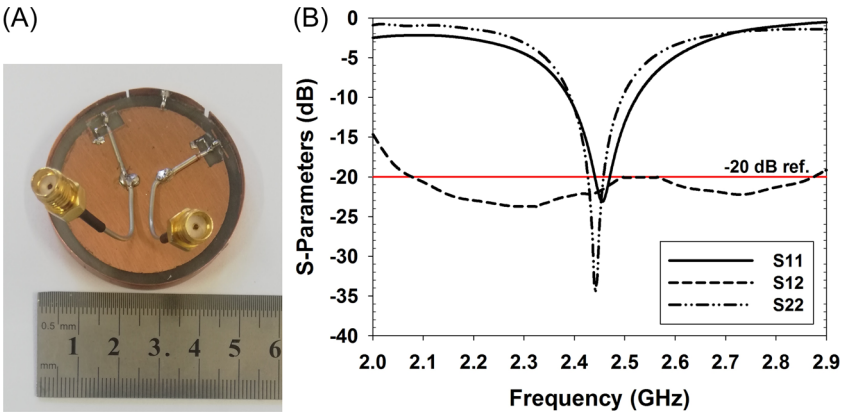

can be observed that the L_c can be used to fine-tune the isolation at the target frequency.

4 | MEASURED RESULTS

The proposed design was fabricated as shown in Figure 4A. The values of L_{r1}, C_{r1}, L_{r2}, C_{f2}, and L_c were 5 nH, 0.55 pF, 6 nH, 0.6 pF, and 3 nH, respectively. The measured S-parameters are presented in Figure 4B. The measured impedance bandwidth (−10 dB) of Antennas 1 and 2 were 130 MHz (2.39–2.52 GHz) and 120 MHz (2.39–2.51 GHz), respectively. The measured isolation bandwidth with reference to −20 dB was 790 MHz (2.08–2.87 GHz). Minor deviation in measured and simulated results occurred due to the fabrication tolerance. The radiation patterns of both antennas were measured in an anechoic chamber with dimensions $9 \times 4.5 \times 4.9\ m^3$. The radiation pattern of each antenna element was measured by exciting one of the antenna elements and terminating the other one with a matched load. Figure 5 shows the simulated and measured

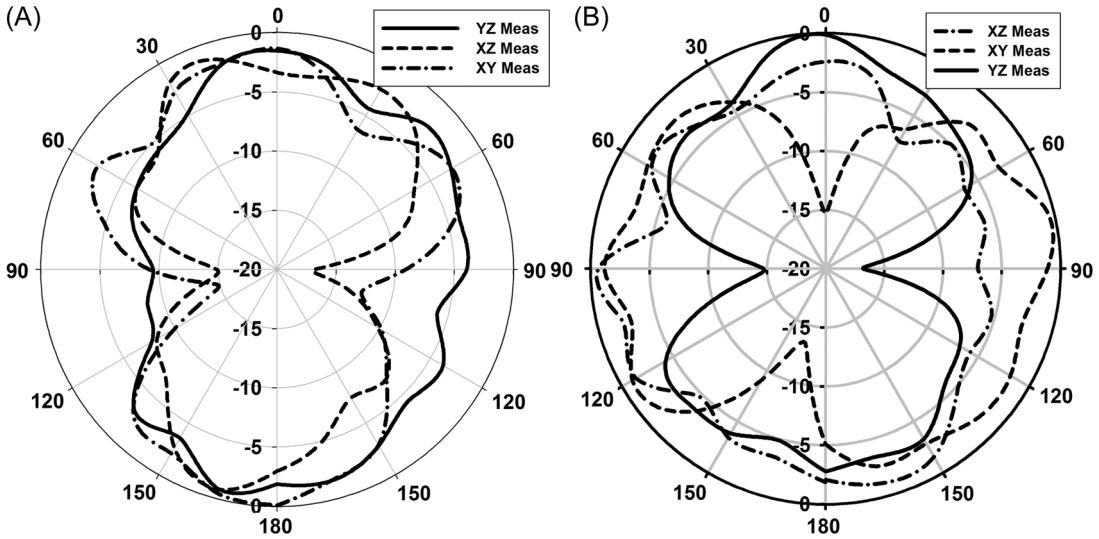

FIGURE 5 Measured radiation patterns when (A) Antenna 1 was excited and (B) Antenna 2 was excited.

radiation pattern of each antenna element. The measured peak gains of Antenna 1 and Antenna 2 were 3.1 and 3.3 dBi, respectively. Envelop correlation coefficient (ECC) expressed by ρ_e is an important figure of merit indicating MIMO performance. The following expression was used to calculate the ECC with the help of measured radiation patterns.[28]

$$\rho_e = \frac{\left|\iint_{4\pi} F_1(\theta,\varphi)F_2(\theta,\varphi)d\Omega\right|^2}{\iint_{4\pi}\left|F_1(\theta,\varphi)\right|^2 d\Omega \iint_{4\pi}\left|F_2(\theta,\varphi)\right|^2 d\Omega}. \quad (3)$$

On excitation of ith port, radiation pattern is represented as F_i (θ, φ). Figure 6 shows the measured and simulated ECC. The measured ECC is well below 0.1 for the entire Wi-Fi band. Figure 7 presents the measured efficiency of antenna elements. The peak values of the efficiencies of Antenna 1 and Antenna 2 are 65.6% and 60.6%, respectively.

The proposed design has been compared with the state-of-the-art literature in Table 1.

The comparison shows that the isolation performance of the proposed antenna is better than.[18–20] However, the performance is lower in comparison with Wen and colleagues.[10,13,14] It is due to the fact that the articles used nonembedded antenna structures. The low-profile antenna structure is a critical demand of modern smart-watch applications. Therefore, the main contribution of the proposed design is that higher isolation bandwidth has been achieved using the coplanar isolator along with the embedded antenna elements within the ground plane.

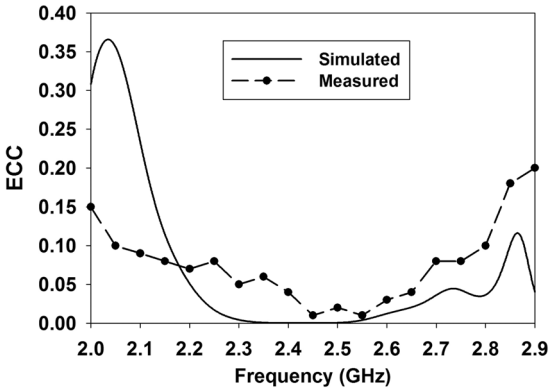

FIGURE 6 Measured and simulated envelop correlation coefficient (ECC) of the proposed antenna.

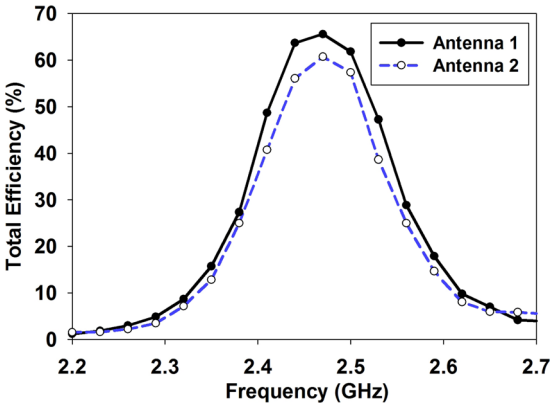

FIGURE 7 Measured total efficiencies of both antenna elements

TABLE 1 Comparison of the proposed design with existing design in literature

References	Type of antenna	Metal frame	Ground dimensions	Operating band (GHz)	Isolation (dB)	Isolation bandwidth (MHz)	Isolation technique
[10]	T-shaped patch	Yes	$\pi 18^2 \times 7$ mm^3	2.4–2.49	>20	>1000	Orthogonal characteristic modes
[13]	Inverted-F antennas	No	$40 \times 40 \times 5.4$ mm^3	2.38–2.52	>20	1000	Larger distance without isolator
[14]	Folded monopole antenna	No	40×40 mm^2	2.9–5.1	>15	1700	Larger slot between antennas
[18]	Ground radiation antenna	Yes	100×50 mm^2	2.4–2.483.5	>14	100	Ground-coupled loop-type isolator
[19]	PIFA antenna	Yes	60×30 mm^2	2.37–2.54	>20	100	T and loop-type isolators
[20]	Ground radiation antenna	No	30×30 mm^2	2.4–2.483.5	>20	600	Circular polarization diversity
This study	T-shaped Ground radiation antenna	Yes	$\pi 26^2 \times 5$ mm^2	2.39–2.52	>20	790	Bezel-coupled loop-type isolator

5 | CONCLUSIONS

In this letter, a wideband isolation technique based on a bezel-coupled T-type isolator has been proposed for smartwatch MIMO applications. The isolator can be controlled by adjusting the bezel gaps and the lumped inductor, and 790 MHz isolation bandwidth is produced by capacitively coupling with the larger bezel. The measured bandwidth of both antenna elements was higher than 110 MHz, and the measured ECC was less than 0.1 over the entire operating band. Meanwhile, the proposed technique is tunable and is not restricted to a specific angular separation between the antenna elements, which makes it a good candidate for the smartwatch MIMO applications.

DATA AVAILABILITY STATEMENT

Data sharing is not applicable to this article as no new data were created or analyzed in this study.

ORCID

Longyue Qu http://orcid.org/0000-0001-5152-091X
Zeeshan Zahid http://orcid.org/0000-0003-2456-0697

REFERENCES

1. Hall PS, Hao Y. *Antennas and Propagation for Body-Centric Wireless Communications*. Artech House; 2012.
2. Chen WS, Lin GQ, Hsu WH. WLAN MIMO antennas with a GPS antenna for smart watch applications. International Workshop on Electromagnetics: Applications and Student Innovation Competition; 2017:89-90. doi:10.1109/iWEM.2017.7968771
3. Jeon M, Choi WC, Yoon YJ. GPS, Bluetooth and Wi-Fi tri-band antenna on metal frame of smartwatch. Proceedings of IEEE International Symposium Antennas Propagation (APSURSI), Fajardo, Puerto Rico; 2016:2177-2178. doi:10.1109/APS.2016.7696795
4. Su S-W, Hsieh Y-T. Integrated metal-frame antenna for smartwatch wearable device. *IEEE Trans Antennas Propag*. 2015;63(7):3301-3305.
5. Wu D, Cheung SW. A cavity-backed annular slot antenna with high efficiency for smartwatches with metallic housing. *IEEE Trans Antennas Propag*. 2017;65(7):3756-3761.
6. Wen D, Hao Y, Wang H, Zhou H. A wearable antenna design using a high impedance surface for all-metal smartwatch applications. Proceedings of International Workshop on Antenna Technology: Small Antennas, Innovative Structures, and Applications (iWAT), Athens, Greece; 2017:274-276.
7. Werner DH, Jiang ZH. *Electromagnetics of Body Area Networks: Antennas, Propagation, and RF Systems*. Wiley Publishers; 2016.
8. Jensen MA, Wallace JW. A review of antennas and propagation for MIMO wireless communications. *IEEE Trans Antennas Propag*. 2004;52(11):2810-2824.
9. Chen Y-S, Ku T-Y. A low-profile wearable antenna using a miniature high impedance surface for smartwatch applications. *IEEE Antennas Wireless Propag Lett*. 2015;15:1144-1147.

10. Wen D, Hao Y, Wang H. Design of a MIMO antenna with high isolation for smartwatch applications using the theory of characteristic modes. *IEEE Trans Antennas Propag*. 2019;67(3):1437-1447.
11. Wang B, Yan S. Design of smartwatch integrated antenna with polarization diversity. *IEEE Access*. 2020;8:123440-123448.
12. Zhang Y, Li Y, Zhang W, Zhang Z, Feng Z. Omnidirectional antenna diversity system for high-speed onboard communications. *Engineering*. 2020;11(4):74-81.
13. Zhang Y, Liu P, Yin Y, Li Y. Omnidirectional dual-polarized antenna using co-located slots with wedgy profile. *IEEE Trans Antennas Propag*. 2021;69(9):5446-5454.
14. Li Y, Zhang Z, Zheng J, Feng Z. Compact azimuthal omnidirectional dual-polarized antenna using highly isolated co-located slots. *IEEE Trans Antennas Propag*. 2012;60(9):4037-4045.
15. Li WW, Zhou JH, Zhang B, You BQ. High isolation dual-port MIMO antenna. *Electron Lett*. 2013;49(15):919-921.
16. Chen W-S, Yang CK, Sin W-S. MIMO antenna with Wi-Fi and Bluetooth for smart watch applications. Proceedings of IEEE MTT-S International Microwave Workshop Series (IMWS), Taipei, Taiwan; 2015:212–213.
17. Woo S, Baek J, Park H, Kim D, Choi J. Design of a compact UWB diversity antenna for WBAN wrist-watch applications. Proceedings of ISAP, Nanjing, China; 2013:1304–1306.
18. Cho O, Choi H, Kim H. Loop-type ground antenna using capacitor. *Electron Lett*. 2011;47(1):11-12.
19. Liu Y, Lu X, Jang H, Choi H, Jung K, Kim H. Loop-type ground antenna using resonated loop feeding, intended for mobile devices. *Electron Lett*. 2011;47(7):426-427.
20. Zahid Z, Kim H. Analysis of loop type ground radiation antenna using equivalent circuit model, IET microwaves. *Antennas Propag*. 2017;11(1):23-28.
21. Qu L, Zhang R, Kim H. Decoupling between ground radiation antennas with ground coupled loop-type isolator for WLAN applications. *IET Microw Antennas Propag*. 2016;10(5):546-552.
22. Zahid Z, Kim H. Decoupler design for MIMO antennas of USB dongle applications using ground mode coupling analysis. *Prog Electromagn Res*. 2018;76:113-122.
23. Qu L, Piao H, Qu Y, Kim H-H, Kim H. Circularly polarised MIMO ground radiation antennas for wearable devices. *Electron Lett*. 2018;54(4):189-190.
24. Shin H, Jeon J, Kim H. Efficiency enhancement of wideband mobile antenna. *Electron Lett*. 2016;53(3):179-181.
25. Hassan M, Zahid Z, Khan AA, Maqsood M. A wideband loop-type ground radiation antenna using ground mode tuning and optimum impedance level. *Microwave Optical Tech Lett*. 2019;61:2056-2061.
26. Pozar DM. *Microwave Engineering*. 4th ed. John Wiley & Sons, Inc; 2011.
27. Harrington RF. *Time Harmonic Electromagnetics*. 2nd ed. Wiley IEEE Press; 2001.
28. Vaughan RG, Andersen JB. Antenna diversity in mobile communications. *IEEE Trans Veh Technol*. 1987;36(4):149-172.

How to cite this article: Baloch BA, Qu L, Zahid Z, Khan AA. A wideband isolation technique using bezel coupled T-type isolator for smartwatch MIMO applications. *Microw Opt Technol Lett*. 2022;64:1984-1990. doi:10.1002/mop.33415